Recent and Future Activities at Leibniz University Hannover in GNSS Frequency Transfer

Thomas Krawinkel
Institut für Erdmessung
Leibniz Universität Hannover
Hannover, Germany
krawinkel@ife.uni-hannover.de

Steffen Schön
Institut für Erdmessung
Leibniz Universität Hannover
Hannover, Germany
schoen@ife.uni-hannover.de

Andreas Bauch
Dept. Time and Frequency
Physikalisch-Technische Bundesanstalt
Braunschweig, Germany
andreas.bauch@ptb.de

***Abstract*—Frequency transfer (FT) based on Global Navigation Satellite System (GNSS) precise point positioning (PPP) enables global comparison of local time scales that are each connected to a GNSS receiver. We use our in-house PPP software to examine the current limits of this technique and extend the classical analysis approach to new GPS and Galileo signals. We also investigate the impact of receiver clock modeling (RCM). For this, we carried out a dedicated experiment at Germany's national metrology institute, the Physikalisch-Technische Bundesanstalt (PTB), where four geodetic receivers – operating in a controlled environment – were connected to one single GNSS antenna and the same UTC(PTB) signal. The link instability of two receivers of the same type is better as compared with the use of receivers of different types. Overall, Galileo signals lead to better FT performance than GPS signals. When using the latter, with modern L2C signals we obtain FT instabilities that are at least comparable to those based on legacy L2 P-code observations. The application of RCM especially improves the short-term link instability. Therefore, this should be studied more in-depth in the future since it can be a valuable approach in GNSS-based FT.**

***Index Terms*—GNSS, frequency transfer, precise point positioning, Allan deviation, clock modeling**

I. Introduction

Today, frequency transfer (FT) based on Global Navigation Satellite System (GNSS) measurements is a standard technique [1], [2]. The preferred primary analysis method is precise point positioning (PPP) [3]. It enables global comparison and distribution of local time scales that are connected to a GNSS receiver. Within the frame of the Collaborative Research Centre *TerraQ (Relativistic and Quantum-based Geodesy)*, it is our goal to push the limits of GNSS FT to the 10^{-17} instability range.

As a first step, we want to explore the minimum achievable frequency link instability between two GNSS receivers, from a technical standpoint. This means to investigate which performance is attainable and what is the noise floor, respecticely, with modern, state-of-the-art GNSS equipment. For this, we carried out a dedicated experiment at the Physikalisch-Technische Bundesanstalt (PTB), Germany's national metrology insitute. The recorded data are analyzed with our in-house PPP software to examine the current limits of this technique. Also, we extend the standard analysis approach, which typically uses legacy GPS L1 and L2 P-code and carrier phase observations, by including new GPS and Galileo signals. Finally, we investigate the impact of receiver clock modeling (RCM) on the FT performance as well.

Funded by the Deutsche Forschungsgemeinschaft (DFG, German Research Foundation) – Project ID 434617780 – SFB 1464.

II. Experiment

For an overall duration of approximately three weeks, from April 20 to May 10, 2021, we conducted a GNSS measurement campaign in a controlled environment at PTB with a total of four modern geodetic GNSS receivers. The latter were placed in a laboratory, where temperature and humidity were steered to certain conditions. These ambient atmosphere values were recorded by a data logger and are shown in Fig. 1. It can be seen that the temperature stayed virtually constant around a mean of 22.9 °C. Note that on the day with the larger deviation in the middle of the campaign (April 30, 2021) no data was recorded. The reason for this – and probably also for the deviation itself – is the fact that on said day we changed the measurement configuration of the experiment. Regarding the relative humidity time series, the conditions were steered around a mean of 50%, i.e. once the upper threshold of roughly 55% was reached they were reduced to about 45%.

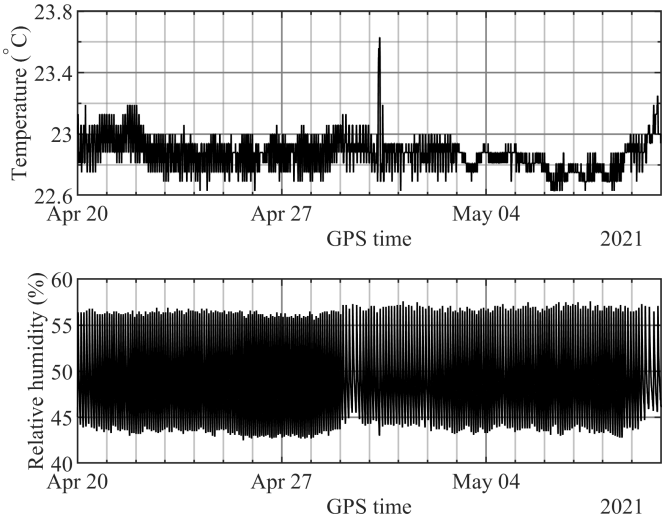

Fig. 1. Temperature and relative humidity data recorded inside the laboratory during the whole experiment.

978-1-6654-3935-0/21/$31.00 ©2021 IEEE

We used four GNSS receivers, two of the same type each, namely two JAVAD OMEGA and two Septentrio PolaRx5TR. At all times, they were connected to the locally generated approximation of Coordinated Universal Time (UTC), referred to as UTC(PTB), by means of a 10 MHz signal. Hence, we call this a common-clock measurement configuration.

The experiment as a whole was split into two parts. At first, in the period April 20–29, all four receivers were connected to one single antenna, which was a Leica AR20 with radome, via an active signal splitter. Such a measurement configuration is usually referred to as zero baseline. In the second part, two receivers, one of each type, were detached from the antenna and connected to another identical one – installed quite exactly two meters away. The antennas were mounted on top of the Meitner building on the PTB campus, and the laboratory with the receivers was located right below on the top floor of that building. Impressions of the measurement environment are shown in Figure 2. In order to ensure similar signal delays from the antenna to all receivers, we used identical cables and connectors from the active signal splitter onward. Each receiver recorded GPS, GLONASS, Galileo, and Beidou signals with a data rate of 1 Hz.

III. Data Analysis

In this contribution, we will focus on the first part of the experiment, i.e. the zero-baseline measurements, as described in section II. We use our in-house MATLAB-based GNSS toolbox to analyze the GPS and Galileo observation data with a sampling interval of 300 s. The reference coordinates of the antenna were determined beforehand with the Leica Infinity software (version 3.4.3) relative to the nearby station PTBB, which is designated as an official fiducial station of the EUREF Permanent GNSS Network [4].

The PPP software is based on a linearized Kalman filter (LKF) with a fixed-interval smoother using ionosphere-free code and carrier phase observations [5]. We apply an elevation-dependent observation weighting scheme based on observation weights

$$w_i = \sqrt{\sin(E_i)} \tag{1}$$

with elevation angle E_i of the i-th satellite. The corresponding elevation cutoff angle amounts to 15°. For reasons of consistency, we then also use this low cutoff angle for all other GNSS observation types. In order to be able to use GPS and Galileo observations in a consistent way, we apply final satellite orbit and clock products computed within the frame of the Multi-GNSS Experiment (MGEX) project by the Centre National d'Etudes Spatiales, Collecte Localisation Satellites (CNES/CLS), [6]–[8]. Furthermore, we make use of the Vienna Mapping Function 3 (VMF3) troposphere model, for both a-priori observation corrections and estimation of the residual effect [9]. We apply satellite-specific differential code biases (DCBs) as provided by the German Aerospace Center (DLR) to the code observations [10]. The carrier phase observations are corrected for satellite and receiver phase center offset and variations, as well as the carrier phase wind-up effect. Finally, various tidal and loading effects are also taken into account during the computations.

Since we are analyzing static GNSS data, the receiver coordinates are estimated as a random constant process. The same applies to the float carrier phase ambiguities. The residual tropospheric zenith delay is estimated by means of a random walk process with a spectral amplitude of $3\,\mathrm{mm}/\sqrt{\mathrm{hour}}$.

The behavior of the receiver clock is assessed by means of the process noise model according to [11]:

$$Q_{\omega\omega} = \begin{bmatrix} q_{11} & q_{12} \\ q_{21} & q_{22} \end{bmatrix}, \tag{2}$$

with

$$q_{11} = \frac{h_0}{2}\Delta t + 2h_{-1}\Delta t^2 + \frac{2}{3}\pi^2 h_{-2}\Delta t^3\,, \tag{3}$$

$$q_{12} = q_{21} = h_{-1}\Delta t + \pi^2 h_{-2}\Delta t^2\,, \tag{4}$$

$$q_{22} = \frac{h_0}{2\Delta t} + 4h_{-1} + \frac{8}{3}\pi^2 h_{-2}\Delta t\,, \tag{5}$$

where Δt is the LKF update interval. The corresponding h_α-coefficients can be calculated, for example, from the Allan deviation (ADEV) of a given oscillator [12], [13]. Generally, process noise values like these are assessed rather relaxed in GNSS data analysis because usually a receiver is driven by its internal temperature compensated crystal oscillator (TCXO). In case the signal of an external oscillator of superior quality, i.e. with better frequency instability, is connected to a receiver, it replaces the internal oscillator signal. In order to take full advantage of such a highly stable signal, the GNSS analysis model has to be adapted accordingly. In an LKF, we do this by applying spectral coefficients appropriate for the superior oscillator in use to the clock process noise model like the one presented in (2). We refer to this approach as receiver clock modeling (RCM) [14]–[16]. The values used in data analysis for a typical TCXO and the UTC(PTB) signal are listed in Table I [17], [18].

Fig. 2. GNSS antennas and receivers atop and inside Meitner building at PTB, respectively. From left to right: first antenna, second antenna, JAVAD OMEGA receivers in the front, Septentrio PolaRx5TR receivers in the back.

IV. Results and Discussion

For all four receivers, we compute the same continuous ten-day PPP solution as described in section III, but with different observation types as listed in Table II. More information about the Receiver Independent Exchange Format (RINEX)

TABLE I
SPECTRAL COEFFICIENTS USED FOR MODELING OF CLOCK PROCESS NOISE

Oscillator / Signal	h_0	h_{-1}	h_{-2}
TCXO	$2 \cdot 10^{-21}$	$1 \cdot 10^{-22}$	$3 \cdot 10^{-24}$
UTC(PTB)	$1.2 \cdot 10^{-26}$	$1.5 \cdot 10^{-30}$	–

observation types can be found in [19]. Note that JAVAD and Septentrio receivers track modern GPS (L2C, L5) and Galileo signals in different ways. However, for reasons of clarity, we generally leave out the corresponding RINEX observation code *attributes*, and only use them to distinguish legacy GPS L2 P-code from modern GPS L2C observations. In order to assess the link instability between two receivers, first, their estimated clock error time series are subtracted from one another. Then, we compute the modified ADEV of this differential time series as a measure for the ultimately achievable instability of frequency comparisons.

The slopes of the ADEV curves in the log-log plots shown in Fig. 3 are approximately $-1/2$, which indicates white frequency noise to be the dominant noise type of the underlying differential clock error time series. All three comparisons show similar behavior regarding the impact of RCM, which especially leads to significantly improved short-term instability. In case of the two *intra*-receiver comparisons shown in Fig. 3a and Fig. 3b, respectively, the curves with and without RCM converge after averaging times of roughly 10^5. On average, RCM improves the link instability about one order of magnitude to the 10^{-18} range after approximately one day averaging time in case of the intra-receiver links.

In contrast to the intra-receiver links, the inter-receiver comparison between a JAVAD and a Septentrio receiver depicted by Fig. 3c shows an overall worse instability. One reason for this are the different tracking modes of both receiver types.

With regard to the various observation type combinations, the performance of the modern GPS L2C signal should be emphasized. Compared to the legacy solution based on L2 P-code observations, they lead to comparable results, although the number of visible satellites is only about 75% (L2C). In case of the JAVAD link (Fig. 3a), the use of L2C in combination with P2-code, i.e. using GPS L2C if satellite transmits it and P2 if not, leads to the best GPS-related instability between the two receivers. Regarding the Galileo solutions, there is virtually no difference visible in the ADEV curves whether we use

TABLE II
OBSERVATION TYPES USED FOR IONOSPHERE-FREE LINEAR COMBINATIONS IN DATA ANALYSIS

Abbreviation	Description
E1-E5	Galileo E1(OS), E5a
E1-E8	Galileo E1(OS), E5(E5a+E5b)
G1-G2W	GPS L1(C/A), L2 (P-code)
G1-G2X	GPS L1(C/A), L2C
G1-G2	GPS L1(C/A), L2 (P-code/L2C)

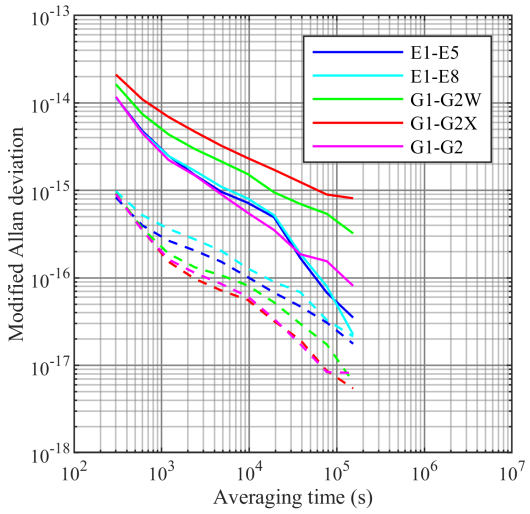

(a) Two JAVAD receivers

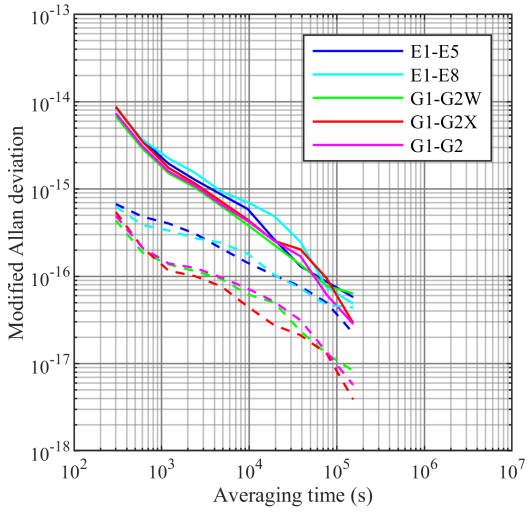

(b) Two Septentrio receivers

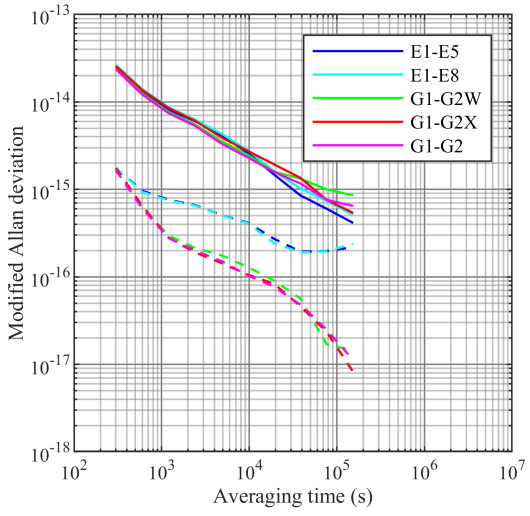

(c) One JAVAD receiver, one Septentrio receiver

Fig. 3. Frequency instability between two GNSS receivers using different ionosphere-free observation type combinations. Dashed lines of the same color indicate corresponding solutions with receiver clock modeling (RCM).

wideband AltBOC (E5a+E5b) observations or simply the E5a signal. Overall, most of the time, the link instability computed from Galileo observations is slightly better as compared to using GPS.

V. Conclusions

This contribution discussed the topic of GNSS frequency transfer using the example of a dedicated measurement campaign carried out in April and May 2021 at Germany's national metrology insitute, the PTB. Four geodetic GNSS receivers, two JAVAD OMEGA and two Septentrio PolaRx5TR, were connected to the highly stable, locally generated UTC(PTB) signal. During the first ten days of the experiment, all receivers were attached to one single Leica AR20 antenna. The recorded data was analyzed by means of a linearized Kalman filter with our in-house PPP software. The same solution was computed using different GPS and Galileo observation types. In addition, each solution was analyzed with and without RCM.

From our results, it was shown that intra-receiver links exhibit better instability values than links based on receivers of different types. Modern Galileo as well as the GPS L2C signal indicate better performance as compared to GPS legacy signals. Using Galileo E5a+b AltBOC instead of E5a signals makes virtually no difference in this case. When applying receiver clock modeling, the link instability gets about one magnitude better into the 10^{-18} range – depending on the signal in use –, especially for short averaging times.

On a final note, one has to keep in mind that all these results originate from a best-case scenario since all receivers were connected to the same antenna. A certain degradation in frequency instability is to be expected when receivers attached to different antennas will be used.

Disclaimer

The authors do not attempt to recommend any of the instruments under test. It is noted that the performance of the equipment presented in this paper depends on the particular environment and the individual instruments in use. Other instruments of the same type or the same manufacturer may show different behavior. The readers are, however, encouraged to test their own equipment to identify the system performance with respect to a particular application.

References

[1] P. Defraigne, "GNSS Time and Frequency Transfer," in *Springer Handbook of Global Navigation Satellite Systems*, P. J. G. Teunissen and O. Montenbruck, Eds., Springer International Publishing, 2017, pp. 1187–1206.

[2] G. Petit, "Sub-10^{-16} accuracy GNSS frequency transfer with IPPP," *GPS Solutions*, vol. 25, no. 1, 2021. DOI: 10.1007/s10291-020-01062-2.

[3] J. F. Zumberge, M. B. Heflin, D. C. Jefferson, M. M. Watkins, and F. H. Webb, "Precise point positioning for the efficient and robust analysis of GPS data from large networks," *Journal of Geophysical Research: Solid Earth*, vol. 102, no. B3, pp. 5005–5017, 1997. DOI: 10.1029/96JB03860.

[4] C. Bruyninx, J. Legrand, A. Fabian, and E. Pottiaux, "GNSS metadata and data validation in the EUREF Permanent Network," *GPS Solutions*, vol. 23, no. 4, 2019. DOI: 10.1007/s10291-019-0880-9.

[5] A. Gelb, J. F. Kasper, R. A. Nash, C. F. Price, and A. A. Sutherland, *Applied Optimal Estimation*. Cambridge, Mass.: MIT Press, 1974.

[6] O. Montenbruck, P. Steigenberger, L. Prange, *et al.*, "The Multi-GNSS Experiment (MGEX) of the International GNSS Service (IGS) – Achievements, prospects and challenges," *Advances in Space Research*, vol. 59, no. 7, pp. 1671–1697, 2017. DOI: 10.1016/j.asr.2017.01.011.

[7] S. Loyer, F. Perosanz, F. Mercier, H. Capdeville, and J.-C. Marty, "Zero-difference GPS ambiguity resolution at CNES-CLS IGS Analysis Center," *Journal of Geodesy*, vol. 86, no. 11, pp. 991–1003, 2012. DOI: 10.1007/s00190-012-0559-2.

[8] G. Katsigianni, S. Loyer, F. Perosanz, *et al.*, "Improving Galileo orbit determination using zero-difference ambiguity fixing in a Multi-GNSS processing," *Advances in Space Research*, vol. 63, no. 9, pp. 2952–2963, 2019. DOI: 10.1016/j.asr.2018.08.035.

[9] D. Landskron and J. Böhm, "VMF3/GPT3: refined discrete and empirical troposphere mapping functions," *Journal of Geodesy*, vol. 92, no. 4, pp. 349–360, 2018. DOI: 10.1007/s00190-017-1066-2.

[10] O. Montenbruck, A. Hauschild, and P. Steigenberger, "Differential Code Bias Estimation using Multi-GNSS Observations and Global Ionosphere Maps," *Navigation*, vol. 61, no. 3, pp. 191–201, 2014. DOI: 10.1002/navi.64.

[11] A. J. van Dierendonck, J. B. McGraw, and R. G. Brown, "Relationship Between Allan Variances and Kalman Filter Parameters," in *Proceedings of the 16th Annual Precise Time and Time Interval Systems and Applications Meeting*, 1984, pp. 273–292.

[12] D. W. Allan, "Time and Frequency (Time-Domain) Characterization, Estimation, and Prediction of Precision Clocks and Oscillators," *IEEE Transactions on Ultrasonics, Ferroelectrics, and Frequency Control*, vol. 34, no. 6, pp. 647–654, 1987.

[13] J. A. Barnes, A. R. Chi, L. S. Cutler, *et al.*, "Characterization of Frequency Stability," *IEEE Transactions on Instrumentation and Measurement*, vol. IM-20, no. 2, pp. 105–120, 1971. DOI: 10.1109/TIM.1971.5570702.

[14] P. Misra, "The role of the clock in a GPS receiver," *GPS World*, vol. 7, no. 4, pp. 60–66, 1996.

[15] U. Weinbach and S. Schön, "GNSS receiver clock modeling when using high-precision oscillators and its impact on PPP," *Advances in Space Research*, vol. 47, no. 2, pp. 229–238, 2011. DOI: 10.1016/j.asr.2010.06.031.

[16] T. Krawinkel and S. Schön, "Benefits of receiver clock modeling in code-based GNSS navigation," *GPS Solutions*, vol. 20, no. 4, pp. 687–701, 2016. DOI: 10.1007/s10291-015-0480-2.

[17] R. G. Brown and P. Y. C. Hwang, *Introduction to Random Signals and Applied Kalman Filtering: With MATLAB Exercises*, 4th edition. J. Wiley & Sons, 2012.

[18] A. Bauch, S. Weyers, D. Piester, E. Staliuniene, and W. Yang, "Generation of UTC(PTB) as a fountain-clock based time scale," *Metrologia*, vol. 49, no. 3, pp. 180–188, Jan. 2012. DOI: 10.1088/0026-1394/49/3/180.

[19] I. Romero, *RINEX: The Receiver Independent Exchange Format Version 3.05*, 2020. [Online]. Available: https://files.igs.org/pub/data/format/rinex305.pdf (visited on 07/16/2021).